Journal of Alloys and Compounds 509 (2011) 4707–4713

Contents lists available at ScienceDirect

Journal of Alloys and Compounds

journal homepage: www.elsevier.com/locate/jallcom

Study on the crystal structure of the rare earth oxyborate $Yb_{26}B_{12}O_{57}$ from powder X-ray and neutron diffraction

Min Yang[a], Kuo Li[a], Jie Su[a], Q. Huang[b], Wei Bao[c], Liping You[d], Zhaofei Li[a], Yingxia Wang[a,*], Yu Jiang[a], Fuhui Liao[a], Jianhua Lin[a,*]

[a] State Key Laboratory of Rare Earth Materials Chemistry and Applications, College of Chemistry and Molecular Engineering, Peking University, Beijing 100871, China
[b] NIST Center for Neutron Research, National Institute of Standards and Technology, Gaithersburg, MD 20899, USA
[c] Department of Physics, Renmin University of China, Beijing 100872, China
[d] Laboratory of Electron Microscopy, Peking University, Beijing 100871, China

ARTICLE INFO

Article history:
Received 12 October 2010
Received in revised form 12 January 2011
Accepted 15 January 2011
Available online 22 January 2011

Keywords:
Rare earth alloys and compounds
Crystal structure
Neutron diffraction
X-ray diffraction
Transmission electron microscopy
Composition fluctuations

ABSTRACT

$Yb_{26}B_{12}O_{57}$, a rare earth oxyborate previously assigned as Yb_3BO_6, has been studied by various techniques including neutron and X-ray diffraction, ^{11}B NMR spectroscopy, electron diffraction and high angle angular dark field-scanning transmission electron microscopy (HADDF-STEM). It crystallizes in the space group C2/m with cell parameters of $a = 24.5780(4)$ Å, $b = 3.58372(5)$ Å, $c = 14.3128(3)$ Å and $\beta = 115.079(1)^\circ$. The structure consists of slabs of rare earth sesquioxide and borate groups. The sesquioxide part is identified from the structural refinement, and is observed from HADDF-STEM image, while elucidation of borate groups is not straightforward. An additional oxygen atom (O31), which links two B_2O_5 groups into a B_4O_{11} polyanion, is identified from the analysis of neutron diffraction data. The occupancy of this oxygen site is only quarter, which results in a random distribution of B_4O_{11} and B_2O_5 groups along the *b*-direction. The chemical formula of ytterbium oxyborate is $Yb_{26}(BO_3)_4(B_2O_5)_2(B_4O_{11})O_{24}$, instead of the simple stoichiometric formula Yb_3BO_6. This compound is paramagnetic but its susceptibility deviated from the Curie–Weiss law at low temperature.

1. Introduction

Recently, rare earth oxyborates have attracted attention due to their potential applications as luminescent materials and fast proton conductors [1–6]. Y_3BO_6:Eu was reported to have high red fluorescence efficiency, comparable with the commercial red phosphors (Y,Gd)BO_3:Eu^{3+} and Y_2O_3:Eu^{3+} [1,2]. Yb^{3+} doped yttrium oxyborate was also used for the spectroscopic studies of Ytterbium [7]. The incorporation of water into lanthanum and neodymium oxyborates enabled these compounds to show fast proton conductive property [3,4]. All of these properties were closely related to the structures of the rare earth oxyborates, and a hard effort has been paid on the structural solutions of rare earth oxyborates [5,6,8–12].

Rare earth oxyborates were initially identified from the phase diagrams of Ln_2O_3–B_2O_3, and their formula was tentatively assigned as Ln_3BO_6 based on preparative phase identification [9,11,12]. These structures were all monoclinic but divided into three different types according to the similarities in their powder X-ray diffraction patterns [11], i.e., the La_3BO_6-type for La–Nd, the Y_3BO_6-type for Sm–Yb and the Lu_3BO_6-type for Lu. Later, the experimental evidence suggested that these rare earth oxyborates were not simple Ln_3BO_6 compounds, but had variable Ln/B ratios in different structure types. Accordingly, the structural details were also complicated [5,6,8,10]. The composition of lanthanum oxyborate was $La_{26}(BO_3)_8O_{27}$ with a La/B ratio significantly higher than 3 (26/8), and its structure contained fluorite-type rare earth oxide slabs and BO_3 groups, [10]. This type of structure was further confirmed by the structural study on its neodymium analogue $Nd_{26}(BO_3)_8O_{27}$ [4]. The Y_3BO_6-type, represented by $Ln_{17.33}(BO_3)_4(B_2O_5)_2O_{16}$ (Ln = Y, Gd), was reported to have a Ln/B ratio of 17.33/8, in which all boron atoms were solely tri-coordinated [5,6,8]. However, the solid state ^{11}B NMR studies revealed the presence of BO_4 groups that challenged the proposed structural model [9]. Besides, the structure of Lu_3BO_6-type oxyborate still remains unknown up to now.

The difficulties for the determination of the structures of rare earth borates are mainly due to the large difference of X-ray scattering abilities between rare earth and boron atoms. Additionally, the structures of borates are often complicated because boron atom can form triangular BO_3 and tetrahedral BO_4 groups with oxygen atoms and these two groups can be isolated, or polymerized to larger anions by sharing oxygen atoms [13]. To obtain the correct structural solution, various techniques including neutron diffraction and spectroscopic characterization need to

* Corresponding authors. Fax: +86 10 627 53541.
E-mail addresses: wangyx@pku.edu.cn (Y. Wang), jhlin@pku.edu.cn (J. Lin).

0925-8388/$ – see front matter © 2011 Elsevier B.V. All rights reserved.
doi:10.1016/j.jallcom.2011.01.098

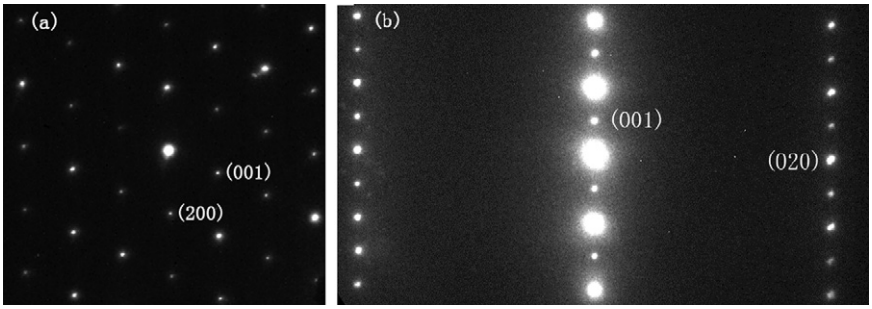

Fig. 1. Electron diffraction of $Yb_{26}B_{12}O_{57}$ along the zone axes (a) [0 1 0], (b) [1 0 0].

be employed. In particular, neutron diffraction is a very powerful tool, as has been demonstrated in determining the structure of YBO_3 [14–16]. In the present work, we report the structural investigation on ytterbium oxyborate using powder X-ray (XRD) and neutron diffraction, infrared (IR) and ^{11}B NMR spectroscopy, and high angle angular dark field-scanning transmission electron microscopy (HADDF-STEM). Ytterbium oxyborate, with a complex formula $Yb_{26}(BO_3)_4(B_2O_5)_2(B_4O_{11})O_{24}$, is identified to belong to the Lu_3BO_6-type structure.

2. Experimental

Polycrystalline samples of all the rare earth (RE) oxyborates were prepared from RE_2O_3 (99.99%) and AR grade H_3BO_3. These starting materials were mixed in an agate mortar, and preheated at 900 °C for 8 h. The samples were reground, pressed into pellets and heated at 1300 °C for 12 h. The above steps were then repeated several times to promote the reaction. A series of samples with different Yb_2O_3/H_3BO_3 ratios were prepared for sieving the product with the proper composition. The samples for neutron diffraction measurement were prepared from boric acid containing solely ^{11}B isotopic boron with a starting Yb/B ratio of 2.125. Lutetium oxyborate was obtained at higher reaction temperature (1500 °C) and thulium oxyborates were prepared at 1300 °C.

Neutron diffraction data were collected at room temperature with a high resolution powder diffractometer BT1, using Cu(3 1 1) monochromator at NIST Center for Neutron Research. Lutetium analogue samples were used for NMR measurements because trivalent ytterbium is paramagnetic. Solid-state ^{11}B NMR spectrum was recorded with a Varian Unity Plus-400 spectrometer at a field of 9.4 T with frequency 128 MHz for ^{11}B, and $BF_3{\cdot}OEt_2$ was used as the reference. Electron diffraction (ED) and HADDF-STEM were carried out using a Tecnai F30 electron microscope. Powder XRD data were collected using a Bruker D8-Advance diffractometer with a curved germanium primary monochromator (Cu Kα1 radiation) in transmission mode (2θ range: 6–120°, step: 0.0144°, scan speed: 30 s/step, 50 kV, 40 mA) at room temperature. Chemical analysis was carried out for ytterbium and boron using Inductively Coupled Plasma (ICP) techniques with an ESCALAB2000 analyzer (samples were dissolved by 6 mol/L HCl and the solution was diluted to meet the demand of ICP analysis). IR spectra were recorded using a Nickel Magna-750 FT-IR spectrometer. Magnetization (M) data were measured with a Quantum Design MPMS XL-5 SQUID system.

3. Results and discussion

3.1. Structure determination

The initial structure model of ytterbium oxyborate was established from XRD data, and its pattern can be readily indexed with a *C*-centered monoclinic cell (Table 1). The systematic absence of XRD reflections ($h+k \neq 2n$) suggested possible space groups of *C*2, *Cm* or *C*2/*m*, which was also confirmed from ED (Fig. 1). To establish the structural model, a full-pattern decomposition program EXTRA was used to extract integrated intensities from the XRD pattern [17]. By refining the lattice constants, background and profile parameters, 962 individual reflection intensities (331 non-overlapping) were obtained in the 2θ range 7–118°. Profile refinement led to a residue value of $R_p = 0.0452$. The structure model was constructed using the direct method with SIRPOW92 [18]. The three possible space groups above were all employed in calculating the structure, and *C*2/*m* was found to be the most suitable space group. The E-map construction revealed seven Yb and thirteen O positions. Phase information of the uncompleted structure was then used to modify the integrated intensities of overlapping reflections, which recovered one additional oxygen and two boron atoms. Another boron atom was identified during construction of the difference Fourier map by Rietveld refinement, which led to a tentative unit cell formula $[Yb_{26}B_{12}O_{56}]^{2+}$. At this stage, all borates were found to be in a triangular geometry (BO_3 or B_2O_5). The Rietveld plots are shown in Fig. S1 in supporting information (SI) and the structure parameters are summarized in Table S1 (SI). Although the refinement proceeded smoothly, unbalanced charge and the presence of a BO_4 group revealed from the ^{11}B NMR spectrum indicated that certain species were missing from the structural model. The Rietveld refinement of the neutron diffraction data enabled us to locate an additional oxygen atom (O31) at the position (0.713, 0, 0.774). O31 was partially occupied (1/4) and located between the triangular planes of BO_3 groups (B3), indicating that these borate groups were randomly distributed BO_3 and BO_4. An additional boron atom (B31, Occ = 1/4) related to B3 was then introduced at the center of the tetrahedron formed by O31 and the three oxygen atoms of the BO_3 group (B3). The final refinement with constrained isotropic temperature factors led to a chemically meaningful structure and low residual factors, $R_p = 0.0344$, $R_{wp} = 0.0408$ and $\chi^2 = 1.50$ (Fig. 2). The composition derived from structural analysis was $Yb_{26}B_{12}O_{57}$. The crystallographic data, refined atomic parameters and bond lengths are listed in Tables 1–3 respectively. Bond angles are given in Table S2 in SI.

3.2. Structure-type and composition of ytterbium oxyborate

The structure of ytterbium oxyborate was previously classified into the Y_3BO_6-type [11]. However, as shown in Fig. 3, the XRD pattern of the ytterbium oxyborate prepared in our study was very similar to that of the Lu_3BO_6-type but significantly different from that of Tm_3BO_6, and the later was classified into the group of Y_3BO_6-type [9,11], It indicated that ytterbium oxyborate should have a

Table 1
Experimental conditions and refinement results for $Yb_{26}B_{12}O_{57}$.

Chemical formula	$Yb_{26}B_{12}O_{57}$
Formula weight	5540.76
Space group	*C*2/*m*
a (Å)	24.5780(4)
b (Å)	3.58372(5)
c (Å)	14.3128(3)
β (°)	115.079(1)
Cell Volume (Å^3)	1141.82(3)
Density (g/cm^3)	8.0607(1)
Temperature	Room temperature
Wavelength of neutron/Å	1.5403
2θ range for extraction	3.0–161°
Preferred orientation (0 1 0)	1.012 (2)
Final *R* indices	$R_p = 0.0344$, $R_{wp} = 0.0408$, $R_{exp} = 0.0272$

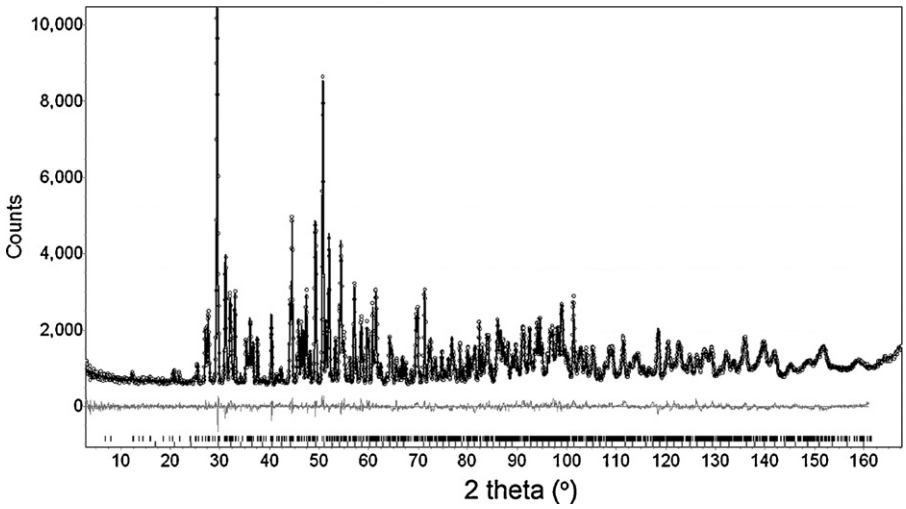

Fig. 2. Rietveld refinement plots for $Yb_{26}B_{12}O_{57}$ by neutron diffraction data. The empty cycles represent the observed data, and the solid line is the calculated pattern. The difference curve is also shown below the diffraction profiles. The upper bars refer to the Bragg reflection positions of $Yb_{26}B_{12}O_{57}$, while the lower bars refer to the Bragg reflection positions of Yb_2O_3 (~11%, w/w).

Lu_3BO_6-type structure other than the previously reported Y_3BO_6-type. To obtain the pure product, a series of samples with Yb/B ratios from 4 to 1.5 in starting materials were prepared. Fig. 4 shows the XRD patterns of four typical samples. The samples from the reactants with higher Yb/B ratio contained a small amount of Yb_2O_3 as impurity, while $YbBO_3$ appeared for the lower Yb/B ratio. A single-phase product was obtained at the ratio of Yb/B = 17/8. The composition of product was affected by the reaction time, owing to evaporative loss of B_2O_3 at high temperature. For example, for the sample containing trace $YbBO_3$ impurity, prolonging the reaction time gradually reduced the $YbBO_3$ content, and eventually might result in the appearance of Yb_2O_3 (Fig. S2 in SI). For the pure sample which was obtained after calcination for 60 h, its Yb/B ratio (2.167) was in agreement with that of the starting material (2.125) and that obtained by chemical analysis (ICP, 2.24 ± 0.09). The composition of the compound, $Yb_{26}B_{12}O_{57}$, was finally established by the structural refinement from neutron diffraction data, and the details about the structure analysis and the refinement results are discussed in the following sections.

3.3. Structure features of $Yb_{26}B_{12}O_{57}$

There are seven ytterbium, fifteen oxygen and four boron atoms in an asymmetric unit of $Yb_{26}B_{12}O_{57}$, as listed in Table 2. Among them, except Yb6 (2*b*) and B31 (general position 8*j*), all the other atoms are located at the special Wyckoff position 4*i* (*x*, 0, *z*), i.e., on the mirror planes at *y* = 0 and 1/2. There are three partially occupied sites, B3 (1/2), B31 (1/4) and O31 (1/4), while the other sites are fully occupied. The projection of the structure along the *b*-direction is shown in Fig. 5a. To emphasize the rare earth oxide parts, Yb and surrounding oxygen atoms have been shadowed. In Fig. 5a, smaller bright parts are BO_3 moieties, and larger ones are B_2O_5 or B_4O_{11}. The HADDF-STEM image of $Yb_{26}B_{12}O_{57}$ along the *b*-direction confirmed these details, as shown in Fig. 5b. The image intensity of a HADDF-

Table 2
Atomic coordinates, occupancies and isotropic thermal displacement parameters of $Yb_{26}B_{12}O_{57}$.

Site	*x*	*y*	*z*	Occupancy	B/Å^2
Yb1	0.8071(2)	1/2	0.6295(3)	1	0.277(23)
Yb2	0.9389(2)	0	0.7569(3)	1	0.277(23)
Yb3	0.9504(2)	1/2	0.5623(3)	1	0.277(23)
Yb4	0.1919(2)	1/2	0.9158(3)	1	0.277(23)
Yb5	0.8473(2)	0	0.8964(3)	1	0.277(23)
Yb6	0	1/2	0	1	0.277(23)
Yb7	0.0824(2)	0	0.6802(3)	1	0.277(23)
O1	0.9884(4)	0	0.6570(6)	1	0.507(31)
O2	0.7924(4)	0	0.9936(7)	1	0.507(31)
O3	0.9494(4)	1/2	0.4081(8)	1	0.507(31)
O4	0.8396(4)	0	0.7317(6)	1	0.507(31)
O5	0.9421(4)	0	0.9165(6)	1	0.507(31)
O6	0.5993(4)	0	0.3392(6)	1	0.507(31)
O7	0.0937(4)	1/2	0.8056(7)	1	0.507(31)
O8	0.0084(4)	1/2	0.8457(6)	1	0.507(31)
O9	0.1087(4)	1/2	0.9798(7)	1	0.507(31)
O10	0.7210(4)	1/2	0.6589(7)	1	0.507(31)
O11	0.6191(4)	1/2	0.5416(6)	1	0.507(31)
O12	0.6850(4)	1/2	0.7909(6)	1	0.507(31)
O13	0.7021(4)	1/2	0.4872(6)	1	0.507(31)
O14	0.7873(3)	1/2	0.8305(6)	1	0.507(31)
B1	0.0710(3)	1/2	0.8789(6)	1	0.268(63)
B2	0.6775(3)	1/2	0.5590(5)	1	0.268(63)
B3	0.7302(4)	1/2	0.7632(6)	1/2	0.268(63)
B31	0.7302(4)	0.406(5)	0.7632(6)	1/4	0.268(63)
O31	0.713(1)	0	0.774(2)	1/4	0.507(31)

Table 3
Bond lengths in $Yb_{26}B_{12}O_{57}$.

Atom	Atom	Distance/Å	Atom	Atom	Distance/Å
Yb1	O6	2.149(10)	Yb2	O5	2.252(10)
	O4	2.236(5) × 2		O1	2.237(12)
	O10	2.326(11)		O6	2.211(5) × 2
	O13	2.395(7) × 2		O4	2.311(10)
	O13	2.520(7)		O8	2.430(5) × 2
		Average: 2.322			Average: 2.297
Yb3	O3	2.196(12)	Yb4	O2	2.149(5) × 2
	O1	2.201(5) × 2		O2	2.237(9)
	O6	2.224(12)		O7	2.255(7)
	O11	2.488(6) × 2		O12	2.485(7) × 2
	O3	2.313(10)		O9	2.572(11)
	O31	2.298(38) × 0.25			Average: 2.332
		Average: 2.302			
Yb5	O4	2.282(10)	Yb7	O3	2.141(5) × 2
	O14	2.257(4) × 2		O1	2.190(10)
	O2	2.314(12)		O12	2.342(8)
	O5	2.222(10)		O7	2.467(7) × 2
	O9	2.429(5) × 2		O11	2.502(11)
		Average: 2.313			Average: 2.321
Yb6	O8	2.304(10) × 2			
	O5	2.286(4) × 4			
	O9	2.806(10) × 2			
		Average: 2.42			
B1	O9	1.352(8)	B2	O10	1.373(8)
	O8	1.394(8)		O13	1.395(11)
	O7	1.385(11)		O11	1.352(10)
B3	O14	1.324(10)	B31	O14	1.366(10)
	O12	1.329(10)		O12	1.371(11)
	O10	1.411(10)		O10	1.451(10)
				O31	1.539(20)

STEM pattern is proportional to Z^2 (Z is the atomic number) [19,20]; thus the bright points correspond to Yb atoms, while B and O atoms reside in the dark areas. The calculated positions of the Yb atoms are superposed on the HADDF-STEM image, which shows that the distribution of Yb atoms fits the image precisely, and an enlarged area containing one unit cell is shown as inset in Fig. 5b.

Among the seven ytterbium atoms, five (Yb1, Yb2, Yb3, Yb5 and Yb7) are seven-coordinated by oxygen atoms, one (Yb6) is eight-coordinated, and one (Yb4) has a variable configuration related to the occupation or the un-occupation of the O31 site. The eight-coordinated Yb6 atom is in a cubic geometry (Fig. 6a), similar to that in the fluorite-type structure. Yb4 is seven-coordinated, when the O31 site is empty; if the O31 site is occupied, an additional bond between Yb4 and O31 (2.3 Å) is formed, and the configuration of Yb4 transforms to eight-coordinated (shown in Fig. 6b). Considering that O31 has only 1/4 occupancy, on average 3/4 of Yb4 atoms are seven-coordinated and 1/4 are eight-coordinated. All the other ytterbium atoms are irregularly seven-coordinated. In Fig. 6c, the coordination polyhedron of Yb7 is shown as an example, and others are given in Fig. S4 in SI. The seven-coordinated polyhedron is common for rare earth atoms as in the sesquioxide Ln_2O_3 structure. The structure of $Yb_{26}B_{12}O_{57}$ can be considered as a combination

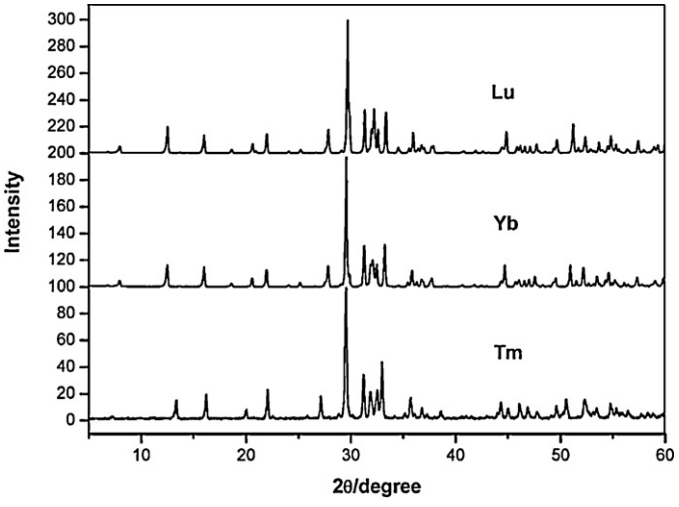

Fig. 3. XRD patterns of Lu, Yb and Tm oxyborates. Yb oxyborate is isostructural to Lu oxyborate, but different from Tm oxyborate (Y_3BO_6-type). The sample of Lu oxyborate contains trace Lu_2O_3 impurity.

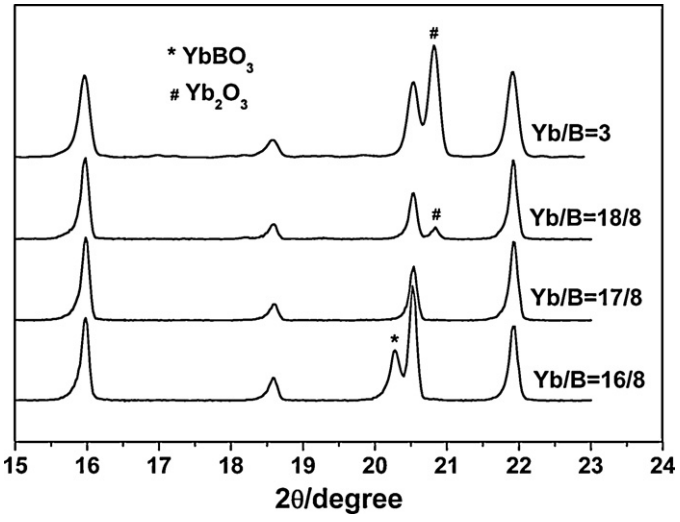

Fig. 4. XRD patterns of Yb-oxyborate samples prepared from different Yb/B ratios. The peak at 20.3° marked by *Corresponds to $YbBO_3$, while that at 20.8° marked by # is due to Yb_2O_3.

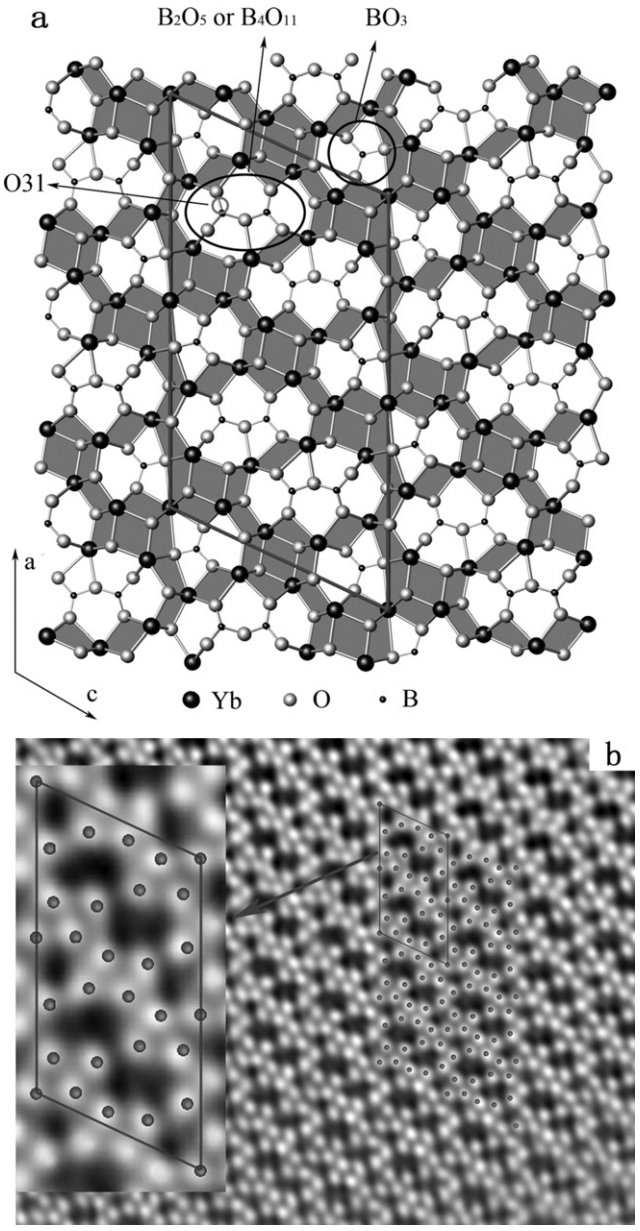

Fig. 5. (a) Projection of the structure of $Yb_{26}B_{12}O_{57}$ along the *b* direction. Large/black balls represent ytterbium, light balls represent oxygen, small black balls represent boron, and the oxide parts of the structure have been shadowed for clarity. (b) HADDF-STEM image of $Yb_{26}B_{12}O_{57}$ along the *b* direction. Bright balls correspond to Yb atoms and dark areas are the positions of borate groups. Superimposed points are Yb positions calculated from the structural model.

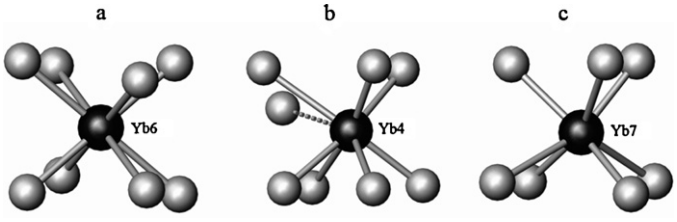

Fig. 6. Coordination polyhedra of (a) Yb6, (b) Yb4 and (c) Yb7.

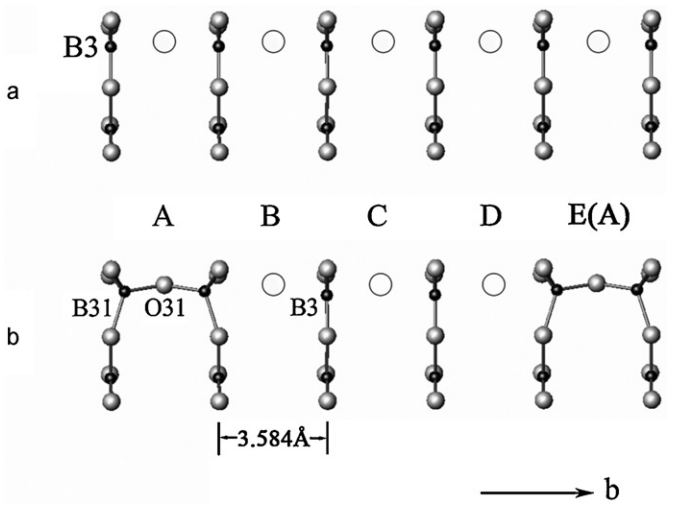

Fig. 7. (a) Distribution of B_2O_5 groups and possible O31 positions along the *b* direction; (b) sketch for the formation of B_4O_{11} groups.

of borate groups and ytterbium sesquioxide slabs. This is different from the structure of lanthanum oxyborate $La_{26}(BO_3)_8O_{27}$ [10], where rare earth oxide parts are predominantly of the fluorite-type.

There are three different borate anions, BO_3^{3-}, $B_2O_5^{4-}$ and $B_4O_{11}^{10-}$ in the structure of $Yb_{26}B_{12}O_{57}$. The isolated triangular borate BO_3^{3-} (B1) is surrounded by eight Yb atoms. From the projection along the *b*-direction, five Yb atoms can be identified (Fig. 5) while the other three are hidden due to the overlap of atoms in the projection. The large dark areas in the HADDF-STEM image correspond to sites filled by B_2O_5 or B_4O_{11} groups. The planar B_2O_5 groups are located on the mirror plan perpendicular to the *b*-direction at $y = 0$ or 1/2, and run parallel in a distance of 3.584 Å, equal to the *b*-parameter of the unit cell. O31 atoms (Occ = 1/4) are at positions between two B3 atoms from two B_2O_5 groups, as shown in Fig. 7a. As a consequence, the insertion of the O31 atom induces the two neighboring boron atoms to shift toward it, giving rise to a tetrahedral configuration, and leading to the formation of B_4O_{11} group, as shown in Fig. 7b. From this structural view, O31 atoms cannot appear in neighboring cells simultaneously. If there is an O31 in position *A*, the next possible positions for O31 are C, D or E but not B (Fig. 7). On average, there is one inserted O31 atom for every four B_2O_5 borate groups. The distribution of B_2O_5 and B_4O_{11} groups along the *b*-direction could be either ordered or random. Since no super-reflections along the *b*-direction were observed (Fig. 1b), this distribution is more likely to be random. The chemical formula of the ytterbium oxyborate can be expressed as $Yb_{26}(BO_3)_4(B_2O_5)_2(B_4O_{11})O_{24}$, in which the B_4O_{11} group consists of two BO_3 and two BO_4 groups, leading to an overall BO_3/BO_4 ratio of 10:2.

The order-disorder distribution of BO_3 and BO_4 groups often occurs in borates. For instances, in boromullites, BO_3 and BO_4 groups are randomly distributed in $Ga_4B_2O_9$ but are ordered in $Al_4B_2O_9$ [21–23]. For the structural determination, such a disorder is not readily apparent from X-ray diffraction data due to the weak scattering ability of boron atom. Thus, great caution should be paid when dealing with the structures of borates. Fortunately, spectroscopic methods such as ^{11}B NMR and IR provide useful information about the local coordination of borate groups. As ytterbium oxyborate is paramagnetic, ^{11}B NMR measurements were carried out on its analogue, lutetium oxyborate, as shown in Fig. 8. The ^{11}B NMR spectrum presents a broad band of several peaks. According to a typical spectrum of BO_3 and BO_4 groups [24], the sharp band at ~0.5 ppm can be attributed to the BO_4 group, while the broad band at 3.2–20 ppm arises from BO_3 resonance. The intensi-

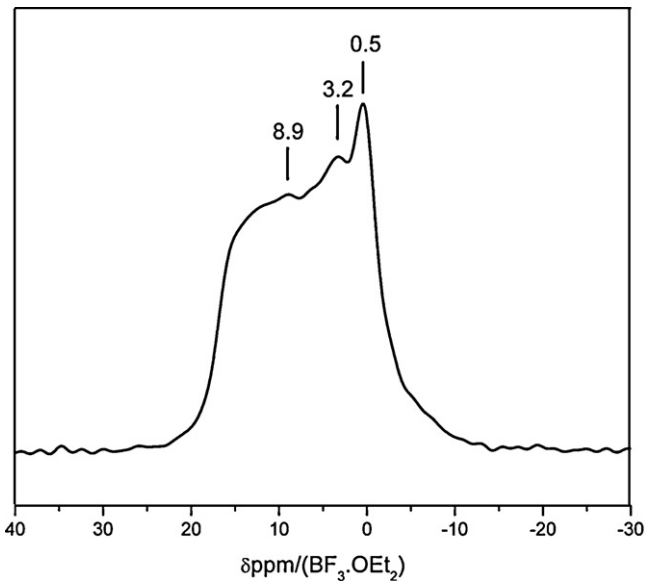

Fig. 8. ^{11}B NMR spectrum of lutetium oxyborate.

ties of the BO_3 and BO_4 signals approximately agree with the ratio of BO_3/BO_4 (10:2) in the structure. The IR spectrum of $Yb_{26}B_{12}O_{57}$ given in Fig. S3 in SI also confirmed the existence of both BO_3 and BO_4 groups.

The structural analysis of $Yb_{26}B_{12}O_{57}$, especially the elucidation of the O31 atom and formation of B_4O_{11} groups, provides a clue in understanding the structure of the yttrium oxyborate. Yttrium oxyborate was initially assigned as Y_3BO_6 [11], but was found to have the composition of $Y_{17.33}(BO_3)_4(B_2O_5)_2O_{16}$ [6]. In this composition, a metal deficient structural model was proposed from XRD and ED data, and all boron atoms are triangularly coordinated. However, ^{11}B NMR revealed both BO_3 and BO_4 groups [9], which implied that there were oxygen atoms missing in the previously structural model. If the positions of Y atoms are all fully occupied, a charge-unbalanced formula $[Y_{18}B_8O_{38}]^{2+}$ can be deduced. The study on the structure of $Yb_{26}B_{12}O_{57}$ indicated that the structure of the Y_3BO_6-type oxyborates may be interpreted using a similar borate model. We suggest the possible composition for Y analogous might be $Y_{18}B_8O_{39}$. Neutron diffraction data is necessary for the identification of the missing oxygen atoms in the structure of yttrium oxyborate.

3.4. Magnetic properties of $Yb_{26}B_{12}O_{57}$

The magnetic susceptibility of $Yb_{26}B_{12}O_{57}$ was measured at the temperature range of 2–300 K, under a magnetic field of 5 kOe. Fig. 9a shows the plots of $\chi_m T$ and $1/\chi_m$ versus T. The $1/\chi_m$ curve deviates from the Curie–Weiss law at low temperature. The $\chi_m T$ value gradually increases and approaches a value of ~29.6 $cm^3\ mol^{-1}\ K$ at 300 K. The magnetic ion in $Yb_{26}B_{12}O_{57}$ is Yb^{III}, which has a valence electron configuration of $4f^{13}$, with the low energy levels including the lowest $^2F_{7/2}$ ground multiplet and a $^2F_{5/2}$ excited multiplet at about 10,000 cm^{-1} higher. The $^2F_{5/2}$ excited state has almost no influence on the magnetic properties. The magnetic interaction between the *f*-configuration is relatively weak and its influence can also be ignored. However, the crystal field surrounding Yb^{3+} ions may induce the splitting of the $^2F_{7/2}$ ground state. The deviation from Curie–Weiss law observed for $Yb_{26}B_{12}O_{57}$ may originate from the thermal population of electrons in sublevels of the ground states induced by the crystal-field. In principle, the magnetic susceptibility can be quantitatively interpreted from crystal-field theory [25,26]. However, for $Yb_{26}B_{12}O_{57}$ it

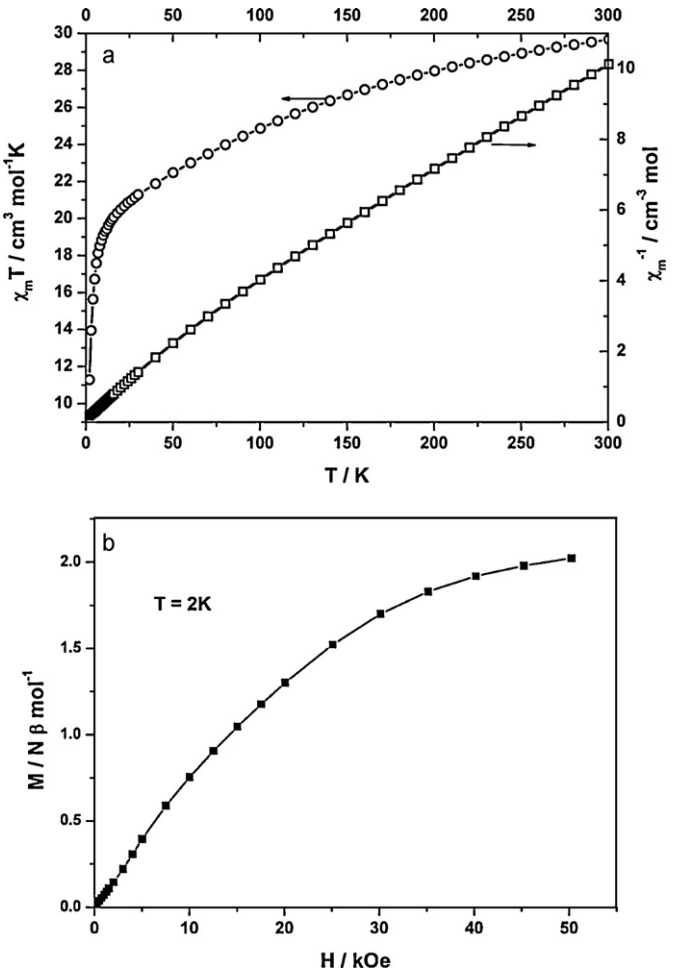

Fig. 9. Magnetic properties of $Yb_{26}B_{12}O_{57}$: (a) temperature dependence of susceptibility, (b) magnetization curve.

is extremely difficult to conduct the quantitative calculations due to the existence of seven different Yb sites in the structure. The field dependence of the magnetization is almost proportional to H at 2 K in the low field region, and shows saturation behavior with the increase of magnetic field (Fig. 9b).

4. Conclusions

Rare earth oxyborates have been known for many years, but there are still many unsolved issues for these materials, including their structures and even compositions. This study clarifies that ytterbium oxyborate crystallizes in the Lu_3BO_6-type structure with a composition of $Yb_{26}B_{12}O_{57}$ other than the simple Yb_3BO_6. Yb atoms are either seven or eight coordinated, and the structure can be regarded as a composite of A-type rare earth oxide slabs and borate groups. There are three kinds of borate groups: BO_3, B_2O_5 and an unusual polyanion B_4O_{11}. B_4O_{11} is formed by the insertion of an oxygen atom (O31) between two adjacent B_2O_5 borates. This quarterly occupied oxygen atom causes the random distribution of B_4O_{11} and B_2O_5 groups along the *b*-direction. The structural analysis of $Yb_{26}B_{12}O_{57}$, especially the elucidation of the O31 atom and formation of B_4O_{11} groups, provides the clue for improving the structure of the yttrium oxyborate and accordingly we proposed a modified formula $Y_{18}B_8O_{39}$ for yttrium oxyborate. Then, we can conclude that the three different rare earth oxyborates, $Ln_{26}(BO_3)_8O_{27}$ ($P2_1/c$) for Ln = La to Nd, $Y_{18}B_8O_{39}$ (Cm) for Ln = Sm to Tm, and $Ln_{26}B_{12}O_{57}$ (C2/m) for Ln = Yb and Lu, all signifi-

cantly deviate from the Ln_3BO_6 composition. They have decreasing Ln/B ratios from 3.25 ($La_{26}(BO_3)_8O_{27}$), to 2.25 ($Y_{18}B_8O_{39}$), and finally to 2.167 ($Yb_{26}B_{12}O_{57}$). Further investigation on the structure of yttrium oxyborate by neutron and NMR techniques is ongoing, and a modified structure model will be presented in the future.

Acknowledgements

Financial support was received from the National Natural Science Foundation of China (20821091), and the State Science and Technology Commission of China (2010CB833103).

Appendix A. Supplementary data

Supplementary data associated with this article can be found, in the online version, at doi:10.1016/j.jallcom.2011.01.098.

References

[1] C. Wang, B. Yan, J. Non-Cryst. Solids 354 (2008) 962–969.
[2] D. Boyer, G. Bertrand-Chadeyron, R. Mahiou, A. Brioude, J. Mugnier, Opt. Mater. 24 (2003) 35–41.
[3] S. Noirault, S. Celerier, O. Joubert, M.T. Caldes, Y. Piffard, Adv. Mater. 19 (2007) 867–870.
[4] S. Noirault, S. Celerier, O. Joubert, M.T. Caldes, Y. Piffard, Inorg. Chem. 46 (2007) 9961–9967.
[5] J.H. Lin, L.P. You, G.X. Lu, L.Q. Yang, M.Z. Su, J. Mater. Chem. 8 (1998) 1051–1054.
[6] J.H. Lin, S. Zhou, L.Q. Yang, G.Q. Yao, M.Z. Su, L.P. You, J. Solid State Chem. 134 (1997) 158–163.
[7] V. Jubera, J. Sablayrolles, F. Guillen, R. Decourt, M. Couzi, A. Garcia, Opt. Commun. 282 (2009) 53–59.
[8] J.H. Lin, Y.X. Wang, L.Y. Li, in: G. Meyer, D. Naumann, L. Wesemann (Eds.), Inorganic Chemistry Highlights, II, WILEY-VCH, Weinheim, 2005, pp. 293–317.
[9] M.T. Cohen-Adad, O. Aloui-Lebbou, C. Goutaudier, G. Panczer, C. Dujardin, C. Pedrini, P. Florian, D. Massiot, F. Gerard, C. Kappenstein, J. Solid State Chem. 154 (2000) 204–213.
[10] J.H. Lin, M.Z. Su, K. Wurst, E. Schweda, J. Solid State Chem. 126 (1996) 287–291.
[11] S.F. Bartram, in: K.S. Vorres (Ed.), Proceedings of the 3rd Conference on Rare Earth Research, (1963), Clearwater, FL, Gordon and Breach, New York, 1964, pp. 165–180.
[12] E.M. Levin, C.R. Robbins, J.L. Waring, J. Am. Ceram. Soc. 44 (1961) 87–91.
[13] A.F. Wells, Structural Inorganic Chemistry, Oxford University Press, London, 1975, 851-862.
[14] J.H. Lin, D. Sheptyakov, Y.X. Wang, P. Allenspach, Chem. Mater. 16 (2004) 2418–2424.
[15] M. Ren, J.H. Lin, Y. Dong, L.Q. Yang, M.Z. Su, L.P. You, Chem. Mater. 11 (1999) 1576–1580.
[16] G. Chadeyron, M. ElGhozzi, R. Mahiou, A. Arbus, J.C. Cousseins, J. Solid State Chem. 128 (1997) 261–266.
[17] A. Altomare, M.C. Burla, G. Cascarano, G. Giacovazzo, A. Guagliardi, A.G.G. Moliterni, G. Polidori, J. Appl. Crystallogr. 28 (1995) 842–846.
[18] A. Altomare, M.C. Burla, M. Camalli, B. Carrozzini, G.L. Cascarano, C. Giacovazzo, A. Guagliardi, A.G.G. Moliterni, G. Polidori, R. Rizzi, J. Appl. Crystallogr. 32 (1999) 339–340.
[19] S.J. Pennycook, D.E. Jesson, Phys. Rev. Lett. 64 (1990) 938–941.
[20] I. Arslan, N.D. Browning, Microsc. Res. Tech. 69 (2006) 330–342.
[21] K.J. Griesser, A. Beran, D. Voll, H. Schneider, Mineral. Petrol. 92 (2008) 309–320.
[22] D. Mazza, M. Vallino, G. Busca, J. Am. Ceram. Soc. 75 (1992) 1929–1934.
[23] R.H. Cong, T. Yang, K. Li, H.M. Li, L.P. You, F.H. Liao, Y.X. Wang, J.H. Lin, Acta Crystallogr. Sect. B: Struct. Sci. 66 (2010) 141–150.
[24] J.C.C. Chan, M. Bertmer, H. Eckert, J. Am. Chem. Soc. 121 (1999) 5238–5248.
[25] J.H. Lin, E. Hey-Hawkins, H.G. von Schnering, Z. Naturforsch. 45a (1990) 1241–1247.
[26] N. Taira, Y. Hinatsu, J. Solid State Chem. 150 (2000) 31–35.